One-dimensional Ising model with long-range and random short-range interactions

A. P. Vieira[†] **and L. L. Gonçalves**[‡]
Departamento de Física da UFC, Cx. Postal 6030
60451-970 Fortaleza (CE), Brazil
[†] Present address: Instituto de Física da USP, 05315-970 São Paulo (SP), Brazil.
[†] E-mail: apvieira@if.usp.br
[‡] E-mail: lindberg@fisica.ufc.br

February 1, 2008

Abstract

The one-dimensional Ising model in an external magnetic field with uniform long-range interactions and random short-range interactions satisfying bimodal annealed distributions is studied. This generalizes the random model discussed by Paladin *et al.* (J. Phys. I France 4, 1994, p. 1597). Exact results are obtained for the thermodynamic functions at arbitrary temperatures, and special attention is given to the induced and spontaneous magnetization. At low temperatures the system can exist in a "ferrimagnetic" phase with magnetization $0 < \sigma < 1$, in addition to the usual paramagnetic, ferromagnetic and antiferromagnetic phases. For a fixed distribution of the random variables the system presents up to three tricritical points for different intensities of the long-range interactions. Field-temperature diagrams can present up to four critical points.

1 Introduction

The one-dimensional Ising model with nearest-neighbor and uniform infinite-range interactions was introduced by Nagle [1] and presents interesting behaviour such as the existence of first- and second-order paramagnetic transitions. The crossover between short- and long-range interactions in the model was later reexamined by Kislinsky and Yukalov [2], and the study of the model for arbitrary interactions was presented by Vieira and Gonçalves [3]. The model is equivalent to a linear chain approximation of higher-dimensional models, and it has been successfully applied to the study of quasi-one-dimensional materials [4, 5].

The presence of infinite-range interactions is responsible for the existence of ferromagnetic ordering at finite temperatures, and is expected to induce even richer behaviour in the presence of disorder. This is confirmed by the analysis of the quenched site-dilute system by Slotte [6], who found that the system exhibits 11 topologically different field-temperature phase diagrams as p and α are varied, where p is the dilution concentration and α measures the ratio between the intensities of nearest-neighbor and infinite-range interactions. Recently, Paladin *et al.* [7] studied a random version of the model, at zero field, in which nearest-neighbor interactions can assume opposite values $\pm J$ with equal probability. In the quenched limit they showed that, as α is varied, infinitely many "ferrimagnetic" ground state phases, with average

spontaneous magnetization $0 < \sigma_0 \leq 1$, are observed. Because of the difficulties involved in the mathematical treatment of the system at arbitrary temperatures, they also considered the annealed limit, which presents simpler ground state behaviour, but where a ferrimagnetic phase is still present.

In a recent paper [8] the present authors considered a generalization of the annealed model studied by Paladin *et al.* by introducing an external field and random nearest-neighbor interactions which satisfy bimodal annealed distributions. The exact solution of the model was presented, and results for the bond-dilute case were briefly discussed. This paper considerably extends the results of the previous one by considering all possible cases for the distribution of the random variables. The exact solution of the model is reviewed in Sec. 2 by using the approach of Thorpe and Beeman [9], which maps the system onto a regular Ising model with an effective temperature dependent interaction. The ground state properties of the system are discussed in Sec. 3, and it is shown that ferrimagnetic phases do appear for a very large range of distributions. At finite temperature the system presents a very rich behaviour, with many phases, as discussed in Sec. 4. Finally, in Sec. 5 the main results of the paper are summarized.

2 The model

Consider a closed-chain (N sites) Ising model in an external magnetic field with uniform long-range interactions and random nearest-neighbor (n.n.) interactions satisfying the bimodal annealed distribution

$$\wp(\kappa_j) = p\delta(\kappa_j - J_A) + (1-p)\delta(\kappa_j - J_B). \tag{1}$$

The Hamiltonian of the model is written as

$$H = -\sum_{j=1}^{N} \kappa_j \sigma_j \sigma_{j+1} - \frac{I}{N} \sum_{i,j=1}^{N} \sigma_i \sigma_j - h \sum_{j=1}^{N} \sigma_j, \tag{2}$$

which generalizes both the pure model [1, 2, 3] and the random model studied by Paladin et al. [7], corresponding to $h = 0$, $J_A = -J_B = J$ and $p = \frac{1}{2}$.

The exact solution of the model was given by the present authors in a previous paper [8], where an even more general model was considered, for which long-range interactions satisfy a strongly correlated distribution. Alternatively, the thermodynamic functions of the model can be easily obtained from the general approach of Thorpe and Beeman [9]. This consists of performing the partial trace over the disorder variables, mapping the system onto a regular Ising model with an effective n.n. interaction K, whose properties are well known [1, 2, 3]. For the random system, the free energy per spin as a function of the average magnetization σ is given by

$$f_a(\sigma) = f(K,\sigma) - k_B T \left\{ p \ln\left[\cosh(K - \beta J_A) - \epsilon(K)\sinh(K - \beta J_A)\right] + \right.$$

$$\left. + (1-p)\ln\left[\cosh(K - \beta J_B) - \epsilon(K)\sinh(K - \beta J_B)\right] - \left[p\ln p + (1-p)\ln(1-p)\right] \right\}, \tag{3}$$

where

$$f(K,\sigma) = -k_B T \ln\left\{ e^K \left[\cosh\tilde{h} + \left(\sinh^2\tilde{h} + e^{-4K} \right)^{1/2} \right] \right\} + I\sigma^2, \tag{4}$$

with

$$\tilde{h} = \beta h + 2\beta I\sigma \equiv \bar{h} + 2\bar{I}\sigma, \tag{5}$$

is the free energy of the regular model [3] with (uniform) effective n.n. interaction K, determined from the solution of the equation

$$\frac{p}{\coth(K-\beta J_A)-\epsilon(K)}+\frac{1-p}{\coth(K-\beta J_B)-\epsilon(K)}=0, \tag{6}$$

and

$$\epsilon(K)\equiv\langle\sigma_j\sigma_{j+1}\rangle_K=1-\frac{2e^{-4K}\left(\sinh^2\tilde{h}+e^{-4K}\right)^{-1/2}}{\cosh\tilde{h}+\left(\sinh^2\tilde{h}+e^{-4K}\right)^{1/2}} \tag{7}$$

is the nearest-neighbor spin-spin correlation function of the regular model. As usual T is the absolute temperature, k_B is Boltzmann's constant and $\beta^{-1}=k_BT$. The equilibrium value of the average magnetization σ is that which minimizes $f_a(\sigma)$, whose relative extrema are determined from the solution of

$$\left(\frac{\partial f_a}{\partial\sigma}\right)_{h,T}=0\Rightarrow$$

$$\Rightarrow\sigma=\frac{\sinh\tilde{h}}{\left(\sinh^2\tilde{h}+e^{-4K}\right)^{1/2}}. \tag{8}$$

The equation of state can be calculated by determining, among the solutions of Eq.8, the absolute minimum of f_a at given field h and temperature T.

Competition between short- and long-range interactions is responsible in the pure model for the existence of first order phase transitions at both zero and non-zero field. It is then natural to expect that it will produce even richer behaviour in the presence of disorder. Assuming the long-range interaction to be ferromagnetic ($I>0$) competition between interactions is obtained by considering J_B bonds as antiferromagnetic ($J_B<0$) and allowing J_A bonds to have arbitrary character ($J_B<J_A<+\infty$). These are the cases considered in this work. As shown for the pure model [3], for $I<0$ the system is fully frustrated and so no spontaneous order is possible even at $T=0$.

3 Ground state properties

Since at $T=0$ the internal energy E and the free energy are equal, the ground state properties of the model can be obtained by looking for those configurations which minimize E for fixed values of the various parameters. For annealed distributions the random variables can adjust themselves so as to minimize the contribution to the free energy due to n.n. interactions, with the sole restriction that the concentration of different kinds of bonds be satisfied. This is in general achieved at fixed average magnetization σ by the formation of interaction domains [9, 7], which avoids frustration effects. On the other hand, the contributions to the internal energy due to long-range interactions I and to the external field h depend only on σ and are given by $-I\sigma^2$ and $-h\sigma$, respectively.

The possible situations are analyzed below.

3.1 Case $J_B<J_A<0$

This is the general case of antiferromagnetic n.n. interactions, due to the symmetry of the model with respect to the transformation $p\to1-p$, $J_A\leftrightarrow J_B$. When both long-range interactions I and field h have

small intensities compared to those of J_A and J_B the system orders antiferromagnetically, satisfying all n.n. bonds. That structure has its energy per site in the thermodynamic limit given by

$$E_{AF} = pJ_A + (1-p)J_B, \tag{9}$$

where p is the concentration of J_A bonds. For intermediate intensities of I and h, ferromagnetic ordering may be induced in the J_A domains, while J_B bonds are still strong enough to maintain local antiferromagnetic ordering. It is easy to verify that such structure has an average magnetization $\sigma = p$, and was called by Paladin *et al.* the "ferrimagnetic" structure [7], whose energy is given by

$$E_{Ferri} = -pJ_A + (1-p)J_B - Ip^2 - hp. \tag{10}$$

For I or h strong enough the system orders ferromagnetically throughout. Such structure, in which no nearest-neighbor bond is satisfied, has unit average magnetization and energy given by

$$E_{Ferro} = -pJ_A - (1-p)J_B - I - h. \tag{11}$$

To determine the range of parameters in which the various structures correspond to equilibrium one has to compare the relative values of E_{AF}, E_{Ferri} and E_{Ferro}. Bearing in mind that for this kind of system σ and h must have the same sign, one finds that the $T = 0$ isotherm is given by

$$|\sigma| = \begin{cases} \begin{cases} 0, \text{ if } 0 < |h| < h_1; \\ p, \text{ if } h_1 < |h| < h_2; \\ 1, \text{ if } |h| > h_2, \end{cases} \text{ for } \begin{cases} J_B < J_A < \frac{1}{2}J_B \text{ and } I < 2(J_A - J_B) \equiv I_{fi} \\ \text{or} \\ J_A > \frac{1}{2}J_B \text{ and } \begin{cases} p < \frac{J_A}{J_B - J_A} \equiv p^* \text{ and } I < I_{fi} \\ \text{or} \\ p > p^* \text{ and } I < -\frac{2}{p}J_A \end{cases} \end{cases} ; \\ \\ \begin{cases} 0, \text{ if } 0 < |h| < h_3; \\ 1, \text{ if } |h| > h_3, \end{cases} \text{ for } \begin{cases} J_B < J_A < \frac{1}{2}J_B \text{ or } J_A > \frac{1}{2}J_B, \ p < p^* \\ \text{and} \\ 2(J_A - J_B) < I < -2[pJ_A + (1-p)J_B] \end{cases} ; \\ \\ \begin{cases} p, \text{ if } 0 < |h| < h_2; \\ 1, \text{ if } |h| > h_2, \end{cases} , \text{ for } J_A > \frac{1}{2}J_B, \ p > p^* \text{ and } -\frac{2}{p}J_A < I < -\frac{2}{1+p}J_B; \\ \\ 1, \text{ if } |h| > 0, \text{ for } \begin{cases} J_B < J_A < \frac{1}{2}J_B \text{ and } I > -2[pJ_A + (1-p)J_B] \\ \text{or} \\ J_A > \frac{1}{2}J_B \text{ and } \begin{cases} p < p^* \text{ and } I > -2[pJ_A + (1-p)J_B] \\ \text{or} \\ p > p^* \text{ and } I > -\frac{2}{1+p}J_B \end{cases} \end{cases} , \end{cases} \tag{12}$$

where

$$\begin{cases} h_1 = -2J_A - pI, \\ h_2 = -2J_B - (1+p)I, \\ h_3 = -2[pJ_A + (1-p)J_B] - I. \end{cases} \tag{13}$$

3.2 Case $J_B < 0 \leq J_A$

In this case, even for $J_A = 0$ and I, $h \to 0^+$ internal energy is minimized by a structure where antiferromagnetic ordering prevails in J_B domains while the rest of the system orders ferromagnetically. This corresponds

to the ferrimagnetic phase ($\sigma = p$), and so for $J_A \geq 0$ there is no stable antiferromagnetic structure. Again for I or h strong enough the system orders ferromagnetically throughout ($\sigma = 1$). The relevant internal energies per spin in the thermodynamic limit are

$$E_{Ferri} = -pJ_A + (1-p)J_B - Ip^2 - hp \tag{14}$$

and

$$E_{Ferro} = -pJ_A - (1-p)J_B - I - h, \tag{15}$$

so that the $T = 0$ isotherm is given by

$$|\sigma| = \begin{cases} \begin{cases} p, & \text{if} \quad 0 < |h| < -2J_B - (1+p)I \\ 1, & \text{if} \quad |h| > -2J_B - (1+p)I \end{cases} , & \text{for} \quad I < -\frac{2J_B}{(1+p)}; \\ \\ 1, \quad \text{if} \quad |h| > 0 \quad \text{for} \quad I > -\frac{2J_B}{(1+p)}. \end{cases} \tag{16}$$

4 Finite temperature properties

From the results of the last section, one concludes that there are essentially three different regimes for the ground state behaviour of the system at zero field, depending on the distribution of the random variables. For $J_B < J_A < \frac{1}{2}J_B$ the spontaneous magnetization ($\sigma_0 \equiv \sigma|_{h=0}$) can assume only the values $\sigma_0 = 0$ and $\sigma_0 = 1$, corresponding to antiferromagnetic and ferromagnetic phases, respectively. For $\frac{1}{2}J_B < J_A < 0$ ferrimagnetic ($\sigma_0 = p$) phases become possible, in addition to antiferromagnetic and ferromagnetic phases. Finally, for $J_A \geq 0$ only ferrimagnetic and ferromagnetic phases exist in equilibrium.

The ground state properties lead to the conclusion that, at finite temperatures, the free energy as a function of σ_0 presents up to five relative minima in the interval $-1 \leq \sigma_0 \leq 1$, corresponding to the symmetric ferromagnetic ($\sigma_0 \simeq \pm 1$) and ferrimagnetic ($\sigma_0 \simeq \pm p$) phases and to the antiferromagnetic (or paramagnetic) phase ($\sigma_0 = 0$). In the presence of an external field $h > 0$ the relative minima of the free energy $f_a(\sigma)$ are shifted towards the positive σ axis and the values of $f_a(\sigma)$ at those minima are altered, which may result in discontinuities or critical points in the $\sigma \times h$ isotherms.

The second order paramagnetic transition temperature T_c is obtained, as in the pure model [3], by taking the $\sigma \to 0$ limit with $h = 0$ in Eq.8, noting however that the effective interaction K depends implicitly on σ through $\epsilon(\sigma)$. Therefore, one obtains

$$e^{-2K_0} \equiv e^{-2K}\big|_{\sigma=0} = 2\beta_c I, \tag{17}$$

where $\beta_c^{-1} = k_B T_c$. Taking the $\sigma \to 0$ limit in Eqs.6 and 7 one also obtains

$$\tanh K_0 = p \tanh(\beta_c J_A) + (1-p)\tanh(\beta_c J_B), \tag{18}$$

and by combining the two previous equations one gets

$$\frac{1 - p\tanh(\beta_c J_A) - (1-p)\tanh(\beta_c J_B)}{1 + p\tanh(\beta_c J_A) + (1-p)\tanh(\beta_c J_B)} = 2\beta_c I, \tag{19}$$

which directly determines T_c.

As discussed for the pure model [3], the tricritical point can be found by solving the system

$$\left.\frac{\partial f_a}{\partial \sigma}\right|_{\sigma=\sigma_t} = 0, \quad f_a(\sigma_t) = f_a(0), \tag{20}$$

and imposing that the $\sigma_t \to 0$ root of the second equation be quadruple by means of a Taylor expansion, which is equivalent to requiring that all derivatives up to fourth order of f_a with respect to σ be zero at $\sigma = 0$. Taking into account the implicit dependence of K on σ, one gets

$$e^{-4K_0} - 3 + 6K_0'' = 0, \tag{21}$$

where

$$K_0'' \equiv \left.\frac{\partial^2 K}{\partial \sigma^2}\right|_{\sigma=0} = -8\,(\beta I)^2\,\frac{p(1-p)\left[\tanh\left(\beta J_A\right) - \tanh\left(\beta J_B\right)\right]^2}{\left\{1 - \left[p\tanh\left(\beta J_A\right) + (1-p)\tanh\left(\beta J_B\right)\right]^2\right\}^2}. \tag{22}$$

For fixed J_A, J_B and p, by solving the system composed of Eqs.18, 21 and 22 the coordinates I_{tr} and T_{tr} of the tricritical point are determined. In the non-random limit ($p = 0$, $p = 1$ or $J_A = J_B$) Eq.22 gives $K_0'' = 0$ and one obtains the pure model result [1, 2, 3]

$$\begin{cases} e^{-2\beta_{tr}J} = 2\beta_{tr} I_{tr}, \\ e^{-4\beta_{tr}J} - 3 = 0. \end{cases} \tag{23}$$

The following subsections analyze the behaviour of the system for different values of J_A and J_B, using the renormalized parameters

$$\delta \equiv \frac{J_A}{J_B}, \quad \alpha \equiv \frac{I}{J_B}, \quad \gamma \equiv \frac{h}{|J_B|}, \quad \theta \equiv \frac{k_B T}{|J_B|}. \tag{24}$$

4.1 Case $J_B < J_A < \frac{1}{2}J_B < 0$ $\left(\frac{1}{2} < \delta < 1\right)$

For this case and at zero field ($h = 0$) the behaviour of the system is qualitatively the same as for the pure model, regardless of the value of p, since there is no stable ferrimagnetic phase. For very strong long-range interactions I the system is ferromagnetic at low temperatures and there is a second order paramagnetic transition. As I gets weaker, passing through the tricritical point $I = I_{tr}$ paramagnetic transitions change to first order and, for $I < I_{ferro} \equiv -2\left[pJ_A + (1-p)J_B\right]$ the ground state becomes antiferromagnetic, and $\sigma_0 = 0$ for all T.

In the presence of a magnetic field $h > 0$ and for $I < I_{fi} \equiv 2(J_A - J_B)$ the $\sigma \times h$ isotherms present two discontinuities at $T = 0$ (from $\sigma = 0$ to $\sigma = p$ and from $\sigma = p$ to $\sigma = 1$), which persist at low temperatures, inducing qualitative differences compared to the pure model. Figures 1(a) and (c) show $\sigma \times \gamma$ isotherms for various values of the renormalized temperature $\theta \equiv k_B T/\left|J_B\right|$ when $\delta = \frac{2}{3}$ and $p = 0.5$, with $\alpha = -0.5$ and $\alpha = -0.6$, respectively, while corresponding $\gamma \times \theta$ phase diagrams are shown in Figs. 1(b) and (d). In both cases there are two discontinuities in the $T = 0$ isotherm for $h > 0$ (or, by symmetry, $h < 0$), producing four first order lines in the phase diagrams. For $\alpha = -0.5$ those lines remain separate, ending at critical points corresponding to temperatures θ_{hc} and θ_{hc}', but for $\alpha = -0.6$ the lines can intersect, giving rise to other two symmetric lines which terminate at a critical point. In fact, one finds that for $\alpha_{hcr2} \simeq -0.5751$ the critical points corresponding to $\theta_{hc}^{'}$ touches the other first order lines, which produces for $\alpha < \alpha_{hcr2}$ the behaviour observed in Figs. 1(c) and (d).

Figure 2 shows the $\theta \times \alpha$ diagram for $\delta = \frac{2}{3}$ and $p = 0.5$. At zero field, as already stated, the behaviour is similar to that of the pure model, with the tricritical point separating regions of first and second order paramagnetic transitions. At non-zero field, on the other hand, there are two critical temperature (θ_{hc}) curves for $\alpha \to 0^-$. One of the curves, as in the pure model, ends at the tricritical point, giving rise to the second order transition temperature θ_c. The other curve ends at point P_{hcr2}, reaching the θ_{hcr3} curve, which touches the α axis at $\alpha_{fi} = -\frac{2}{3}$.

4.2 Case $\frac{1}{2}J_B < J_A < 0$ $(0 < \delta < \frac{1}{2})$

The most interesting kind of behaviour occurs for values of $\delta \in (0, \frac{1}{2})$. The existence of ferrimagnetic phases at zero field for $p > p^* \equiv J_A/(J_B - J_A)$ is responsible for strong qualitative changes in the phase diagrams.

For $p > p^*$ and $I > I_{ferri} \equiv -2J_A/p$ the system can undergo first order ferri-ferromagnetic transitions as the temperature is raised, as observed in the $\theta \times \alpha$ diagrams of Figs. 3 and 4 for $\delta = \frac{1}{3}$ and $p = 0.6$ and $p = 0.7$, respectively. In both figures dotted curves show first-order ferri-ferromagnetic temperatures θ_f. For $p^* = 0.5 < p = 0.6 < p_{cr2} \simeq 0.6596$ there is coexistence of paramagnetic, ferrimagnetic and ferromagnetic phases at point P_{cr3}, where the θ_f curve reach the first-order paramagnetic transition temperature θ_t. So, to the left of P_{cr3} first-order ferri-paramagnetic transition occur at θ_t. On the contrary, for $p = 0.7 > p_{cr2}$ the θ_f curve does not reach θ_t, ending at point P_{cr} together with θ'_{hc}.

The behaviour of the spontaneous magnetization σ_0 can be understood by analyzing the evolution of the free energy $f_a(\sigma_0)$ as the temperature is varied. For $\delta = \frac{1}{3}$ and $p = 0.7$ Figs. 5(a) and (b) show $f(\sigma_0) \equiv f_a(\sigma_0)/|J_B|$ at different temperatures for $\alpha = -1.10 > \alpha_{cr} \simeq -1.1018$ and $\alpha = -1.13$, respectively. In both cases the ground state is antiferromagnetic ($|\sigma_0| = p$) and there exist metastable states for $|\sigma_0| = 1$ and $\sigma_0 = 0$. For $\alpha = -1.10$ the metastable ferromagnetic state disappears at $\theta \simeq 0.2$ and the spontaneous magnetization increases with temperature in a certain range. At $\theta_t \simeq 0.430$ the system undergoes a first order ferri-paramagnetic transition. On the other hand, for $\alpha = -1.13$ first-order ferri-ferromagnetic and ferro-paramagnetic transitions occurs at $\theta_f \simeq 0.115$ and $\theta_t \simeq 0.532$.

Zero field transitions can be better observed in Figs. 6 and 7, which show σ_0 as a function of the renormalized temperature θ for the case $\delta = \frac{1}{3}$ with $p = 0.6$ and $p = 0.7$, respectively. For $p = 0.6$ the ground state is ferromagnetic for $\alpha < \alpha_{ferro} = -1.25$, and the system undergoes first-order ferro-paramagnetic transitions for $\alpha > \alpha_{tr} \simeq -1.6997$. If $\alpha_{ferro} < \alpha < \alpha_{ferri} \simeq -1.1111$ the ground state is ferrimagnetic, and if $\alpha < \alpha_{cr3} \simeq -1.2009$ both first-order ferri-ferromagnetic and ferro-paramagnetic transitions occur. If $\alpha > \alpha_{cr3}$ only first-order ferri-paramagnetic transitions are observed. For $p = 0.7$, when $\alpha_{tr} \simeq -1.4960$, $\alpha_{ferro} \simeq -1.1764$ and $\alpha_{ferri} \simeq -0.9523$, the behaviour is much the same, with the important exception that ferri-ferromagnetic transition occur if $\alpha_{ferro} < \alpha < \alpha_{cr} \simeq -1.1018$, and exactly if $\alpha = \alpha_{cr}$ there is a point in the $\sigma_0 \times \theta$ curve where σ_0 is a continuous function, but its thermal derivative diverges. An important feature of this model that is evident in Fig. 7 is the increase of σ_0 with temperature in a certain range, which is verified in some perovskite-like materials such as $Zn_{1-x}Ga_xMn_3C$ ($x \leq 1$) and $CuMn_3N$ [10]. Finally it should be noted that for $|\alpha|$ greater than what is shown in the figures the behaviour of σ_0 becomes identical to that of the pure model, with the ferro-paramagnetic transition changing from first to second order at the tricritical point.

The effects of the existence of ferrimagnetic phases at zero field on the $\gamma \times \theta$ phase diagrams can be observed for $\delta = \frac{1}{3}$ with $p = 0.6$ and $p = 0.7$ in Figs. 8(a)-(f) and Figs. 9(b) and (d). For $p = 0.6$ figures 8(a)-(f) show the evolution of $\gamma \times \theta$ diagrams from $\alpha = -1$ to $\alpha = -1.21$. If $\alpha > \alpha_{ferri} \simeq -1.1111$ the diagrams are similar to those shown in Fig. 1(b). Exactly at $\alpha = \alpha_{ferri}$ there appears a zero-field first-order line, which splits at $\theta = \theta_f$, giving rise to two symmetric first-order lines. If $\alpha > \alpha_{hcr2} \simeq -1.1295$ symmetric lines intersect at $\theta = \theta_{hcr3}$, and γ_{hcr3}, the corresponding field, becomes zero at $\alpha_{cr3} \simeq -1.2009$. For $p = 0.7$ there is no intersection of symmetric first-order lines, as shown in Figs. 9(b) and (d). Figures 9(c) and (d) illustrate the behaviour of the system if $\alpha = \alpha_{cr}$, when one of the coexistence curves just touches the σ axis.

As the value of δ becomes smaller a reentrant behaviour appears in the ferri-ferromagnetic transition temperature (θ_f) lines, as can be seen in Fig. 10, which shows $\theta \times \alpha$ diagrams at zero field for $\delta = \frac{1}{5}$ and various values of p. The reentrant behaviour of θ_f, evident in Figs. 10(b) and (c), is reflected in the thermal behaviour of the spontaneous magnetization σ_0 shown in Fig. 11, where two first-order ferri-ferromagnetic transition occur for $\alpha_{cr} \simeq -1.3108 < \alpha < \alpha_{re} \simeq -1.2710$. The existence of reentrant behaviour in random

models with competing interactions is common in both annealed [9] and quenched [11] systems.

Reentrant behaviour in $\theta \times \alpha$ diagrams is related to the structure of first-order lines in $\gamma \times \theta$ phase diagrams, as observed in Figs. 12(b) and (d), for $\delta = \frac{1}{5}$, $p = 0.5$, and $\alpha = \alpha_{re} \simeq -1.2710$ and $\alpha = -1.29$, respectively. In the first case the symmetric upper and lower first order lines are tangent to the $\gamma = 0$ axis at $\theta = \theta_{re}$, while in the second case those lines are composed of two distinct segments, touching the $\gamma = 0$ axis at temperatures θ_f and θ'_f, producing the discontinuities observed in the corresponding $\sigma_0(\theta)$ curve in Fig. 11.

For $0 < \delta \lesssim 0.1649$ the $\theta \times \alpha$ diagrams can present up to three tricritical points for $p \in (p'_{rt}, p_{rt})$. This is exemplified for $\delta = 0.16$ and $p'_{rt} \simeq 0.4504 < p = 0.453 < p_{rt} \simeq 0.4567$ in Fig. 13. The existence of three tricritical points (P_{tr}, P'_{tr} and P''_{tr}) is reflected in the appearance of another zero-field second-order paramagnetic transition line for $\alpha''_{tr} < \alpha < \alpha'_{tr}$. That line changes from only one point for $p = p'_{rt}$, where P'_{tr} and P''_{tr} coincide, until it joins the usual θ_c line for $p = p_{rt}$, where P''_{tr} coincides with P_{tr}. An example of $\theta \times \alpha$ diagram with two tricritical points is given in Fig. 14. It should be noted that point P_{c2}, which marks the intersection of the θ_f, θ'_c and θ_t lines, is not a tricritical point, since all those lines correspond to $h = 0$, and so the critical exponents at P_{c2} have the usual mean-field values ($\alpha = 0$, $\beta = \frac{1}{2}$, $\gamma = 1$, $\delta = 3$, within the usual convention of critical indices).

4.3 Case $J_A \geq 0$ ($\delta \leq 0$)

In this situation there is no antiferromagnetic ground state, as discussed in Sec. 3. Irrespective of the value of $\alpha \equiv I/|J_B|$ there is always a second-order ferri- or ferro-paramagnetic transition at a finite temperature. This is illustrated by the $\theta \times \alpha$ diagrams of Figs. 15-17 for $\delta = 0$ and p varying from $p = 0.2$ to $p = 0.4$, where there is at most only one tricritical point. This happens for all $\delta \leq 0$, and the tricritical point exists only for $p < p_{mc}$, where $p_{mc} \to 0$ as $\delta \to -\infty$. Among the cases shown in the figures, the most interesting diagram corresponds to $p = 0.3$, where there are two points P_{c2} and P'_{c2} at which θ_t, θ_f and θ_c lines intersect.

Figures 18 and 19 show $\sigma \times \gamma$ isotherms and $\gamma \times \theta$ phase diagrams for $\delta = 0$ with $p = 0.2$ and $p = 0.3$, respectively. In the first case, Fig. 18(b) shows the $\gamma \times \theta$ diagram for $\alpha = -1.5 > \alpha_{re}$, and three first-order lines are observed, one of which corresponds to $\gamma = 0$. The two remaining symmetrical lines are tangent to each other for $\alpha = \alpha_{re}$, and this gives rise to reentrant behaviour of the spontaneous magnetization for $\alpha < \alpha_{re}$, as previously discussed. For $\alpha = \alpha_{c2} \simeq -1.6549$, as shown in Figs. 18(c) and (d), the critical temperature θ_c of the first-order $\gamma = 0$ line coincides with θ'_f, the temperature at which the symmetrical $\gamma \neq 0$ lines reappear. In the case $p = 0.3$, Figs. 19(b) and (d) exemplify the behaviour of the system around point P'_{c2} (Fig. 16), which marks the reappearance of a critical (second-order) point in the $\gamma = 0$ first-order line. Such critical point is absent for $\alpha'_{c2} < \alpha < \alpha_{c2}$.

5 Conclusions

In this paper the one-dimensional Ising model with uniform infinite-range interactions and random nearest-neighbor interactions in an external field was studied. The random bond κ_i connecting the sites i and $i+1$ was considered to satisfy the bimodal annealed probability distribution

$$\wp(\kappa_j) = p\delta(\kappa_j - J_A) + (1-p)\delta(\kappa_j - J_B).$$

Explicit results were presented for the cases where there is competition between short- and long-range interactions. In order to avoid complete frustration of the system long-range interaction was assumed to be ferromagnetic. Competition was then produced by assuming J_B to be antiferromagnetic and letting J_A be of

arbitrary character. It was shown that at $T = 0$ the system can present antiferromagnetic, ferromagnetic and "ferrimagnetic" ordering. The spontaneous magnetization was shown to present unusual behaviour such as first-order ferri-ferromagnetic transitions, positive thermal derivative and reentrant behaviour. For certain distributions in which $0 < \delta \lesssim 0.1649$, where δ is the ratio between the possible values of antiferromagnetic nearest-neighbor interactions, the system can present up to three tricritical points as the intensity of the infinite-range interactions is varied. Many topologically different field-temperature phase diagrams are possible, and these can present up to four critical points, as opposed to the pure model which presents at most two critical points.

References

[1] J. F. Nagle, Phys. Rev. A **2** (1970) 2124.

[2] V. B. Kislinsky and V. I. Yukalov, J. Phys. A **21** (1988) 227.

[3] A. P. Vieira and L. L. Gonçalves, Cond. Matt. Phys. (Ukraine) **5** (1995) 210.

[4] A. Pires and D. Hone, J. Phys. Soc. Jpn. **44** (1978) 43.

[5] A. V. de Carvalho and S. R. Salinas, J. Phys. Soc. Jpn. **44** (1978) 238.

[6] P. A. Slotte, J. Phys. C **18** (1985) L959.

[7] G. Paladin, M. Pasquini, and M. Serva, J. Phys. I France **4** (1994) 1597.

[8] L. L. Gonçalves and A. P. Vieira, J. Magn. Magn. Mater. **177-181** (1998) 76.

[9] M. F. Thorpe and D. Beeman, Phys. Rev. B **14** (1976) 188.

[10] P. L'Heritier, Ph.D. thesis, INPG, Grenoble, France, 1980.

[11] W. F. Wolff and J. Zittartz, Z. Phys. B **60** (1985) 185.

Figure captions

Figure 1. $\sigma \times \gamma(\gamma \equiv h/|J_B|)$ isotherms (a,c) and $\gamma \times \theta(\theta \equiv k_B T/|J_B|)$ phase diagrams (b,d) for $\delta = \frac{2}{3}$ ($\delta \equiv J_A/J_B$) and $p = 0.5$, with $\alpha = -0.5(\alpha \equiv I/J_B)$ (a,b) and $\alpha = -0.6$ (c,d). Dotted curves in (a) and (c) correspond to phase coexistence boundaries, while full lines in (b) and (d) indicate first order transitions.

Figure 2. $\theta \times \alpha$ diagram for $\delta = \frac{2}{3}$ and $p = 0.5$. The dashed line shows the first order phase transition temperature (θ_t), which intersects the upper solid line corresponding to second order transition temperatures (θ_c for $h = 0$ and θ_{hc} for $h \neq 0$) at the tricritical point P_{tr}. Temperature θ_{hcr3} at which first order lines intersect in $\gamma \times \theta$ diagrams is shown in the dash-dotted curve. Point P_{hcr2} marks the intersection of that curve with another second-order curve. In this and all the following $\theta \times \alpha$ diagrams labels "para" and "ferro" relate to regions in the diagram where at zero field the system is at paramagnetic and ferromagnetic phases, respectively.

Figure 3. The same as in the previous figure for $\delta = \frac{1}{3}$ and $p = 0.6$. Solid and dashed curves represent second and first-order paramagnetic transition temperatures, respectively. The dotted curve shows the first-order ferri-ferromagnetic transition temperature θ_f. At point P_{cr3}, where θ_{hcr3}, θ_f and two θ_t curves intersect, paramagnetic, ferrimagnetic and ferromagnetic phases coexist. The label "ferri" relates to the region where, at zero field, the system is at the ferrimagnetic phase.

Figure 4. The same as in the previous figure for $\delta = \frac{1}{3}$ and $p = 0.7$. Differently from the previous diagram, there is no three-phase coexistence point P_{cr3} nor point P_{hcr3}, since the θ_f curve ends at P_{cr}, reaching the θ'_{hc} curve before reaching the θ_t curve.

Figure 5. Renormalized free energy f ($f \equiv f_a/|J_B|$) as a function of the spontaneous magnetization σ_0 for various temperatures in the case $\delta = \frac{1}{3}$, $p = 0.7$ and $\alpha = -1.10$ (a) and $\alpha = -1.13$ (b).

Figure 6. Spontaneous magnetization σ_0 as a function of the renormalized temperature θ for $\delta = \frac{1}{3}$, $p = 0.6$ and various values of α.

Figure 7. The same as in the previous figure for $\delta = \frac{1}{3}$ and $p = 0.7$. Notice that for $\alpha = \alpha_{cr}$ there is a point in which σ_0 is a continuous function of the temperature but the derivative diverges.

Figure 8. $\gamma \times \theta$ phase diagrams for $\delta = \frac{1}{3}$, $p = 0.6$ and values of α ranging from $\alpha = -1$ (a) to $\alpha = -1.21$ (f).

Figure 9. $\sigma \times \gamma$ isotherms (a,c) and $\gamma \times \theta$ phase diagrams (b,d) for $\delta = \frac{1}{3}$ and $p = 0.7$, with $\alpha = -1$ (a,b) and $\alpha = \alpha_{cr} \simeq -1.1018$ (c,d).

Figure 10. $\theta \times \alpha$ diagrams at zero field for $\delta = \frac{1}{5}$ and $p = 0.4$ (a), $p = 0.48$ (b), $p = 0.5$ (c) and $p = 0.6$ (d). Notice the reentrant behaviour of the first-order ferri-ferromagnetic transition lines, evident in (b) and (c).

Figure 11. Spontaneous magnetization σ_0 as a function of the renormalized temperature θ for $\delta = \frac{1}{5}$, $p = 0.5$ and various values of α.

Figure 12. $\sigma \times \gamma$ isotherms (a,c) and $\gamma \times \theta$ phase diagrams (b,d) for $\delta = \frac{1}{5}$ and $p = 0.5$, with $\alpha = \alpha_{re} \simeq -1.2710$ (a,b) and $\alpha = -1.29$ (c,d).

Figure 13. $\theta \times \alpha$ diagram for $\delta = 0.16$ and $p = 0.453$. Notice the existence of three tricritical points (P_{tr}, P'_{tr} and P''_{tr}) and of another zero-field second-order paramagnetic transition for $\alpha''_{tr} < \alpha < \alpha'_{tr}$. For $\alpha'_{tr} < \alpha < \alpha_{tr}$ there is a third θ_{hc} line just above the θ_t line, but omitted from the figure for clarity.

Figure 14. $\theta \times \alpha$ diagram for $\delta = 0.15$ and $p = 0.42$. The first-order ferri-ferromagnetic transition line (θ_f) intersects the second-order ferri-paramagnetic transition line (θ'_c) and the first-order ferro-paramagnetic transition line (θ_t) at point P_{c2}, which is *not* a tricritical point.

Figure 15. $\theta \times \alpha$ diagram for $\delta = 0$ and $p = 0.2$.

Figure 16. $\theta \times \alpha$ diagram for $\delta = 0$ and $p = 0.3$. The dotted line in the inset corresponds to fist-order ferri-ferromagnetic transition temperatures (θ_f).

Figure 17. $\theta \times \alpha$ diagram for $\delta = 0$ and $p = 0.4$.

Figure 18. $\sigma \times \gamma$ isotherms (a,c) and $\gamma \times \theta$ phase diagrams (b,d) for $\delta = 0$ and $p = 0.2$, with $\alpha = -1.5$ (a,b) and $\alpha = \alpha_{c2} \simeq -1.6549$ (c,d).

Figure 19. $\sigma \times \gamma$ isotherms (a,c) and $\gamma \times \theta$ phase diagrams (b,d) for $\delta = 0$ and $p = 0.2$, with $\alpha = -1.65$ (a,b) and $\alpha = -1.71$ (c,d).

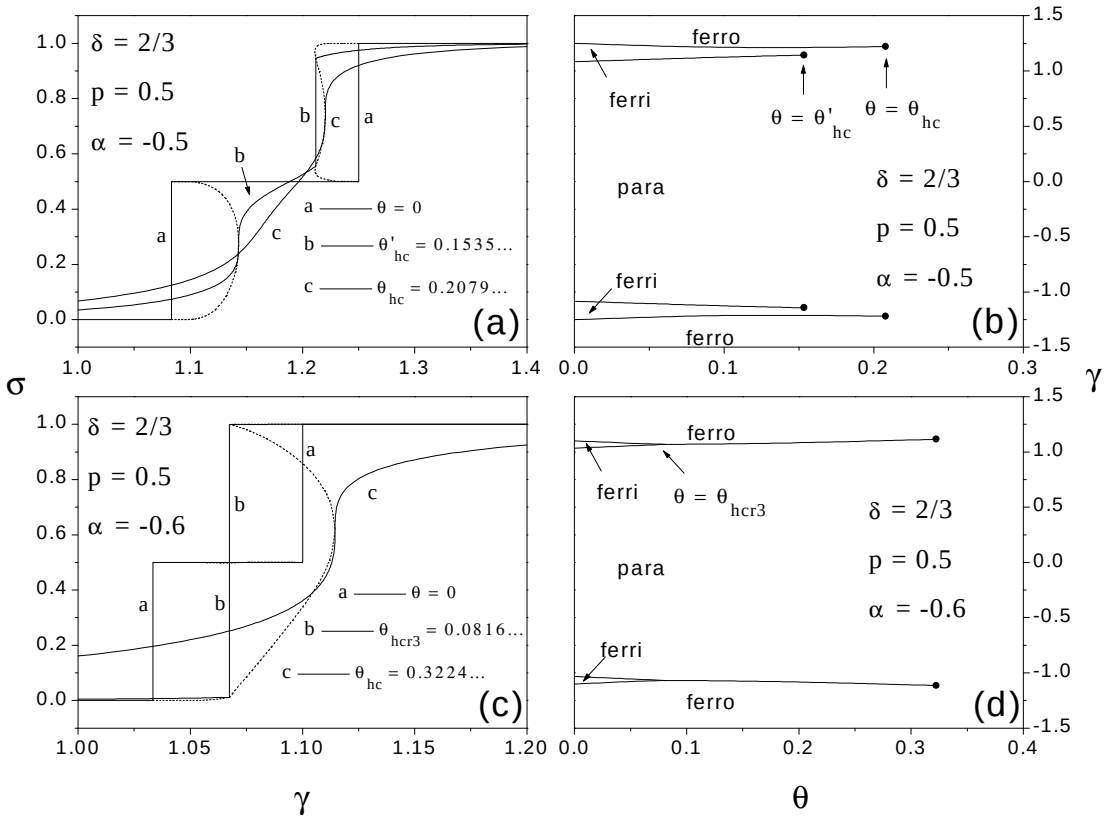
δ = 2/3
p = 0.5
α = -0.5
a —— θ = 0
b —— θ'hc = 0.1535...
c —— θhc = 0.2079...
(a)
ferro
ferri
θ = θ'hc
θ = θhc
para
δ = 2/3
p = 0.5
α = -0.5
ferri
ferro
(b)
σ
γ
δ = 2/3
p = 0.5
α = -0.6
a —— θ = 0
b —— θhcr3 = 0.0816...
c —— θhc = 0.3224...
(c)
ferro
ferri
θ = θhcr3
para
δ = 2/3
p = 0.5
α = -0.6
ferri
ferro
(d)
γ
θ

Figure 1

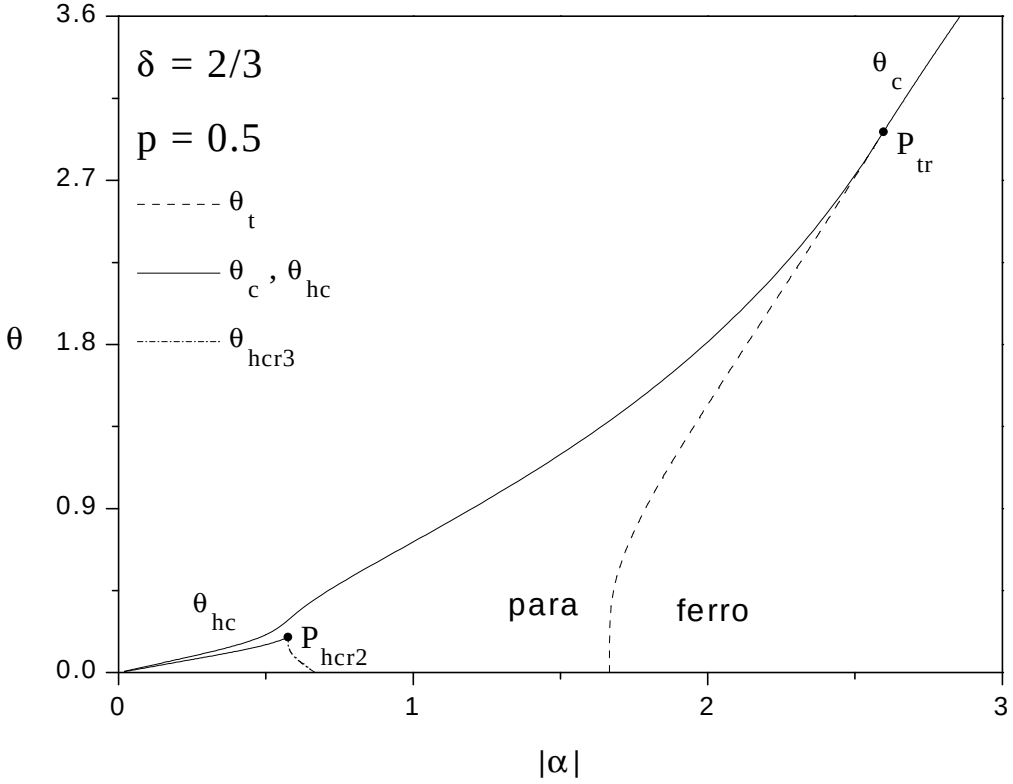
δ = 2/3
p = 0.5
θ t
θ c , θ hc
θ hcr3
θ c
P tr
θ hc
P hcr2
para
ferro
θ
|α|
3.6
2.7
1.8
0.9
0.0
0
1
2
3

Figure 2

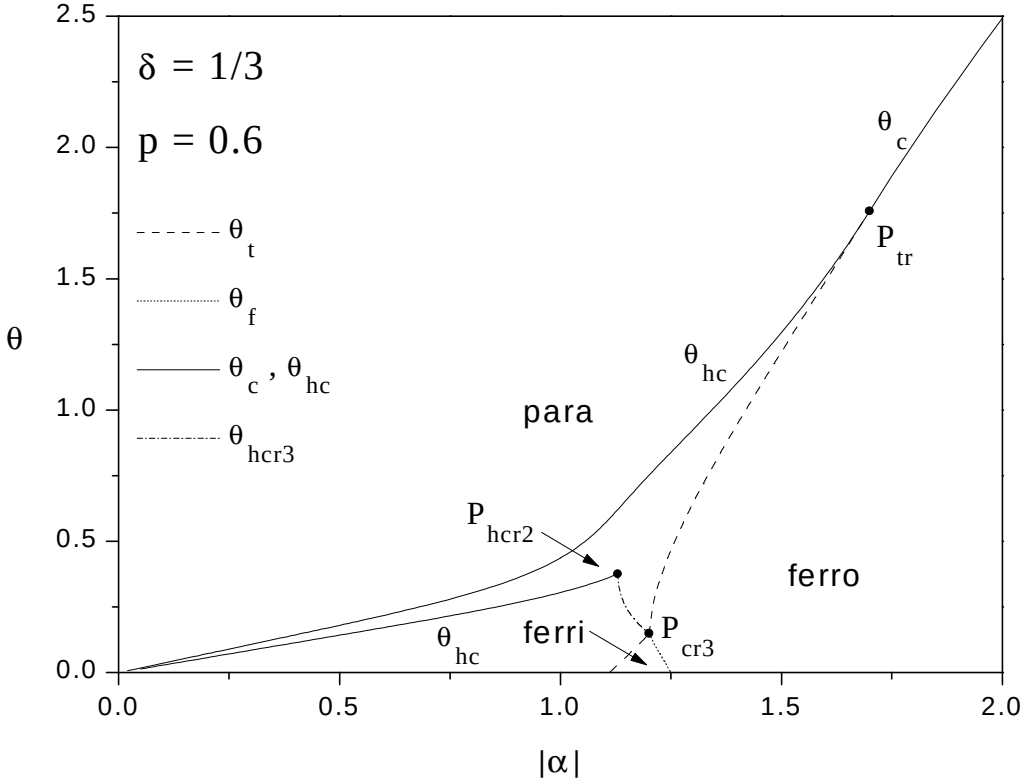
δ = 1/3
p = 0.6
θ t
θ f
θ c , θ hc
θ hcr3
θ c
P tr
θ hc
para
P hcr2
ferro
θ hc
ferri
P cr3
θ
|α|
0.0
0.5
1.0
1.5
2.0
2.5

Figure 3

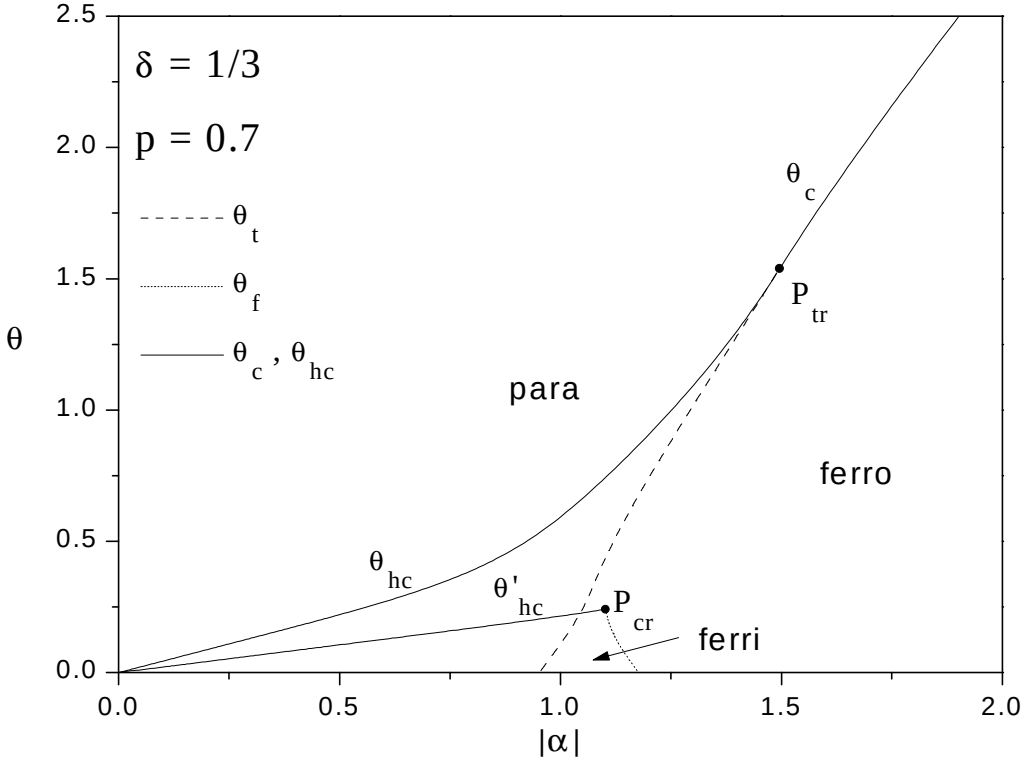
δ = 1/3
p = 0.7
θ t
θ f
θ c , θ hc
θ c
P tr
para
ferro
θ hc
θ' hc
P cr
ferri
θ
|α|
0.0
0.5
1.0
1.5
2.0
2.5

Figure 4

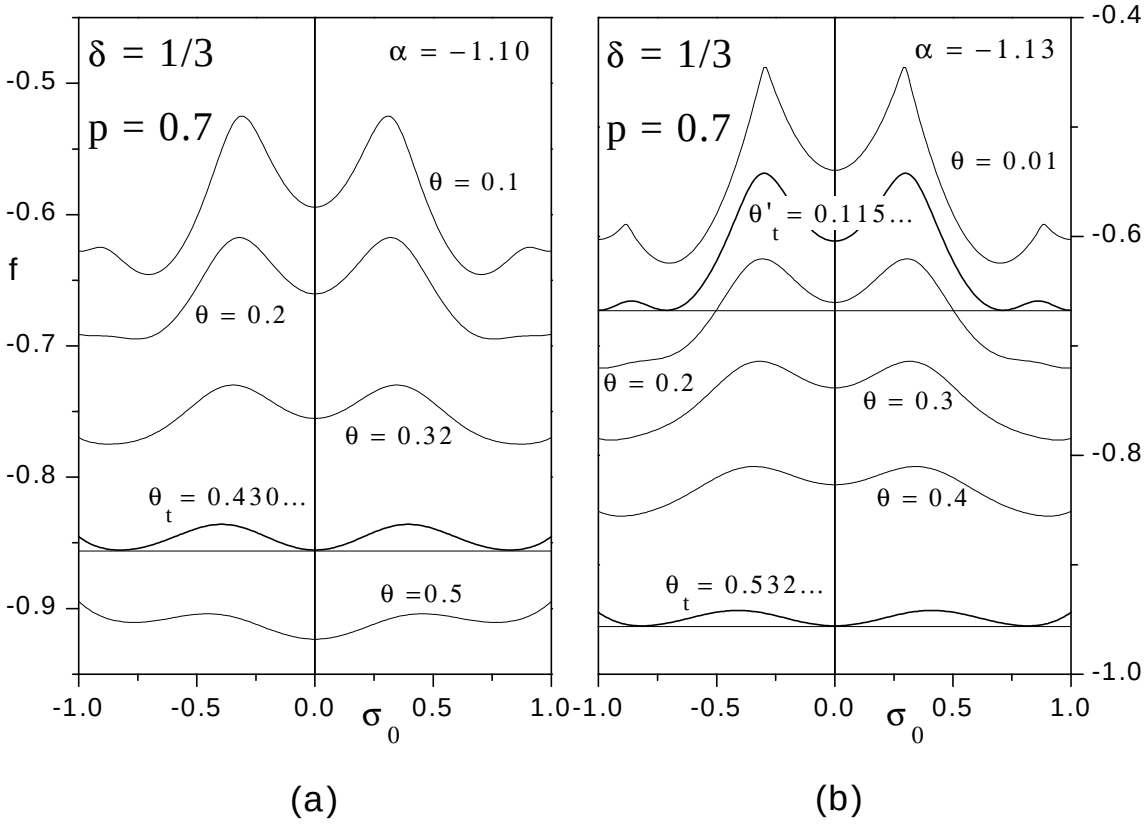
δ = 1/3
p = 0.7
α = −1.10
θ = 0.1
θ = 0.2
θ = 0.32
θ_t = 0.430...
θ =0.5
f
σ_0
(a)
δ = 1/3
p = 0.7
α = −1.13
θ = 0.01
θ'_t = 0.115...
θ = 0.2
θ = 0.3
θ = 0.4
θ_t = 0.532...
σ_0
(b)

Figure 5

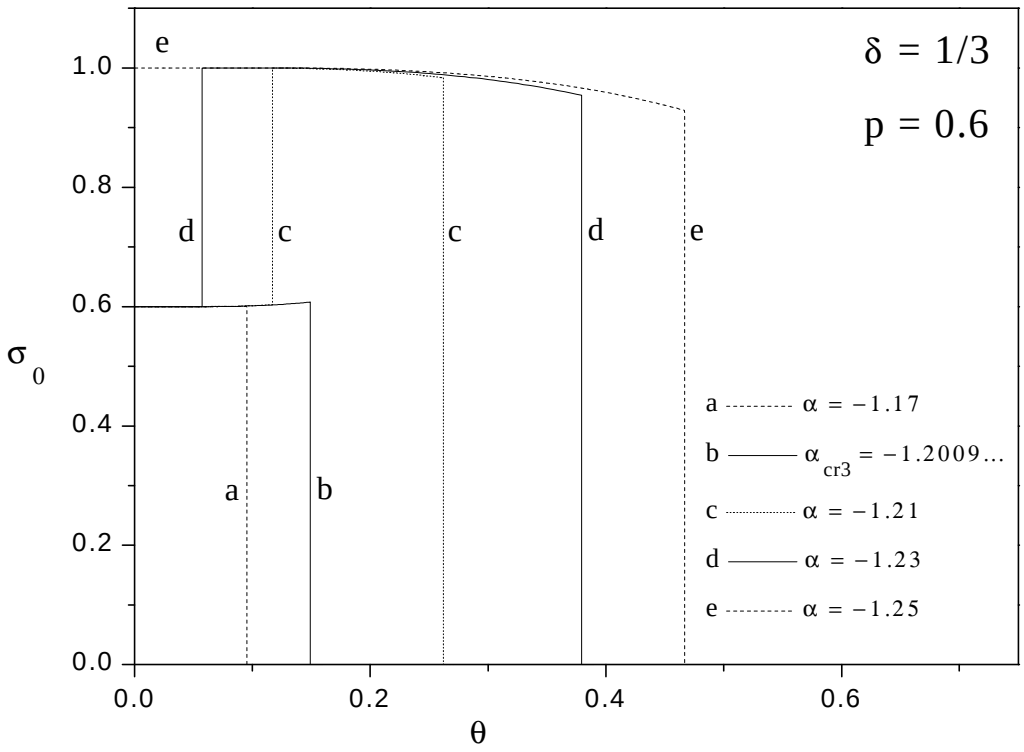
δ = 1/3
p = 0.6
e
d
c
c
d
e
a
b
a ····· α = −1.17
b ——— α cr3 = −1.2009...
c ····· α = −1.21
d ——— α = −1.23
e ····· α = −1.25
σ 0
θ
1.0
0.8
0.6
0.4
0.2
0.0
0.0
0.2
0.4
0.6

Figure 6

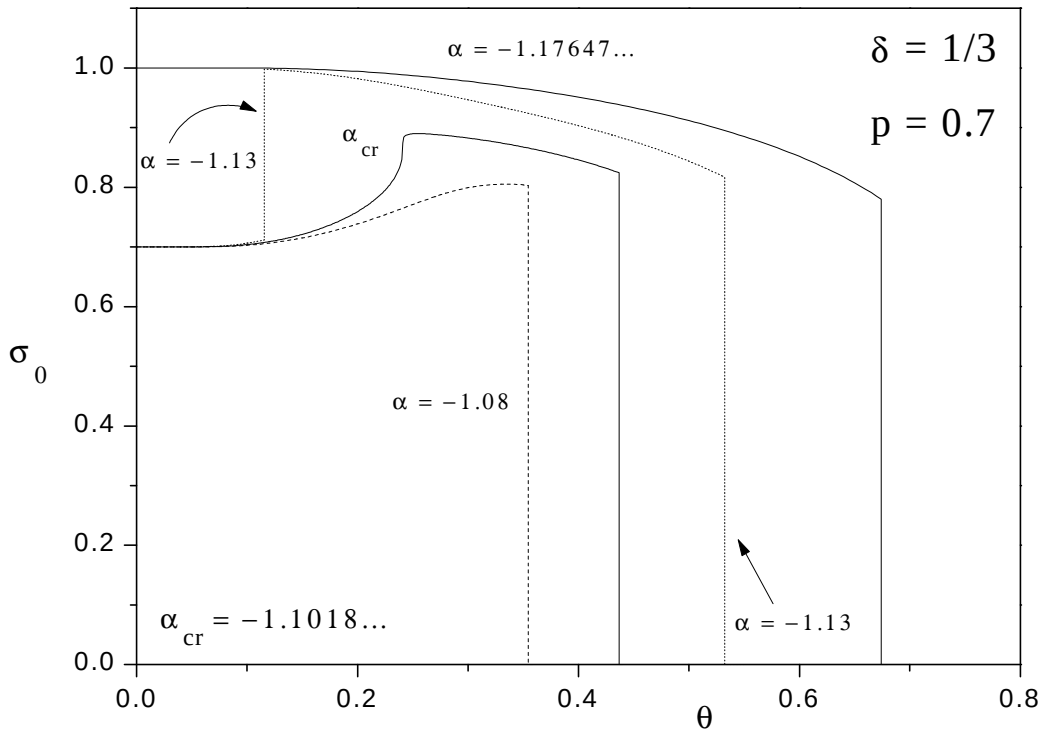
α = −1.17647...
δ = 1/3
p = 0.7
α = −1.13
α cr
α = −1.08
α cr = −1.1018...
α = −1.13
σ 0
θ
1.0
0.8
0.6
0.4
0.2
0.0
0.0
0.2
0.4
0.6
0.8

Figure 7

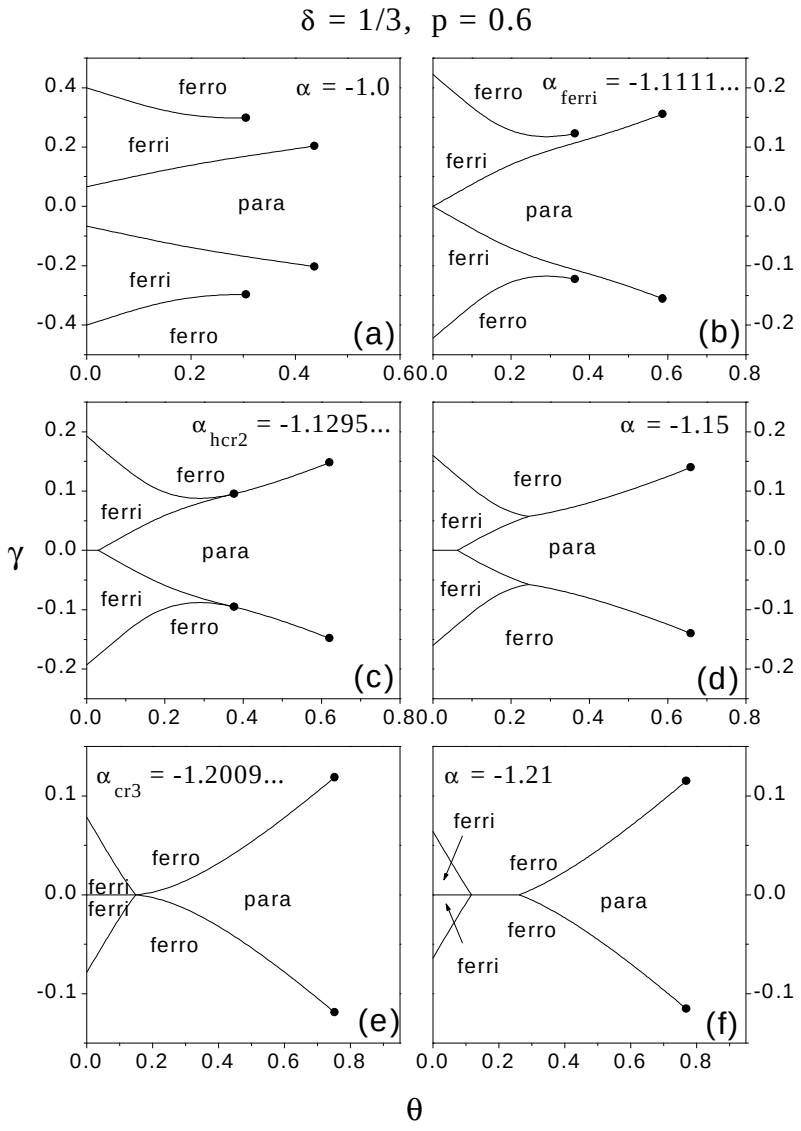
δ = 1/3, p = 0.6
ferro
α = -1.0
ferri
para
ferri
ferro
(a)
ferro
α ferri = -1.1111...
ferri
para
ferri
ferro
(b)
α hcr2 = -1.1295...
ferro
ferri
para
ferri
ferro
(c)
α = -1.15
ferro
ferri
para
ferri
ferro
(d)
α cr3 = -1.2009...
ferro
ferri
ferri
para
ferro
(e)
α = -1.21
ferri
ferro
para
ferro
ferri
(f)
γ
θ

Figure 8

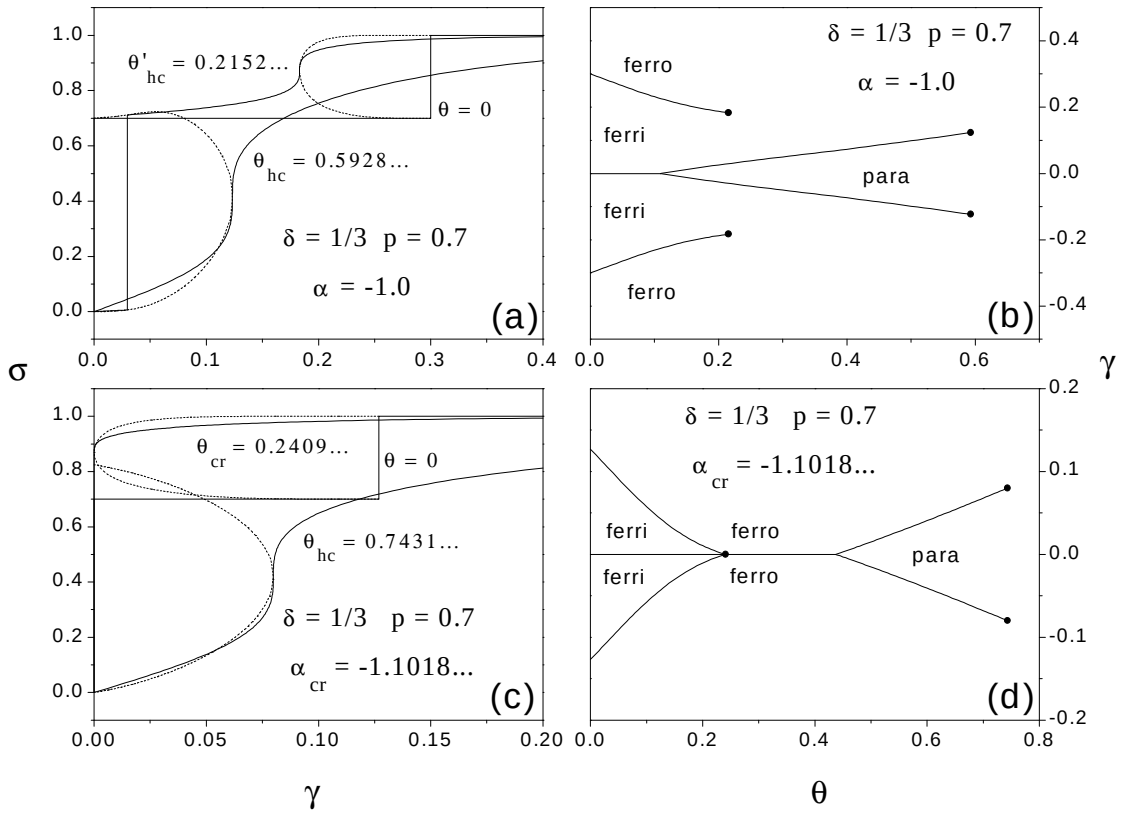
θ'hc = 0.2152...
θ = 0
θhc = 0.5928...
δ = 1/3 p = 0.7
α = -1.0
(a)
δ = 1/3 p = 0.7
α = -1.0
ferro
ferri
para
ferri
ferro
(b)
σ
γ
θcr = 0.2409...
θ = 0
θhc = 0.7431...
δ = 1/3 p = 0.7
αcr = -1.1018...
(c)
δ = 1/3 p = 0.7
αcr = -1.1018...
ferri
ferro
ferri
ferro
para
(d)
γ
θ

Figure 9

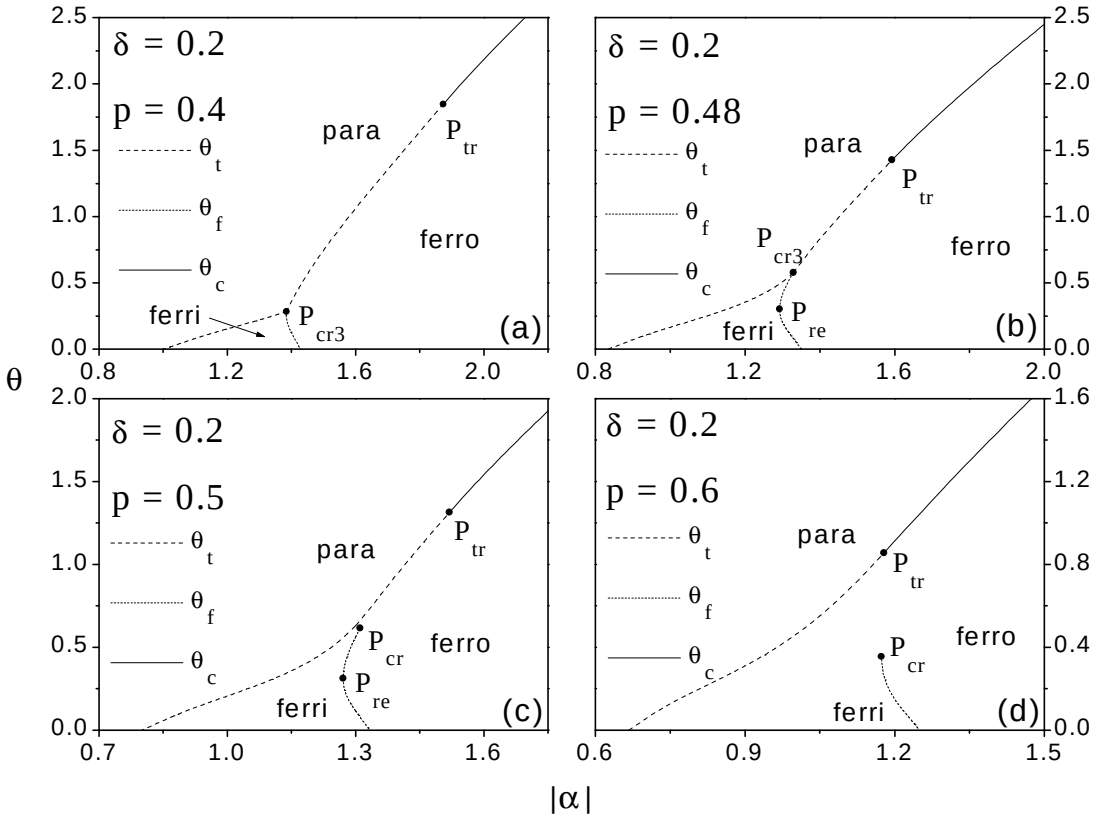
δ = 0.2
p = 0.4
θ t
θ f
θ c
para
ferro
ferri
P tr
P cr3
(a)
δ = 0.2
p = 0.48
P cr3
P re
(b)
δ = 0.2
p = 0.5
P cr
(c)
δ = 0.2
p = 0.6
(d)
θ
|α|

Figure 10

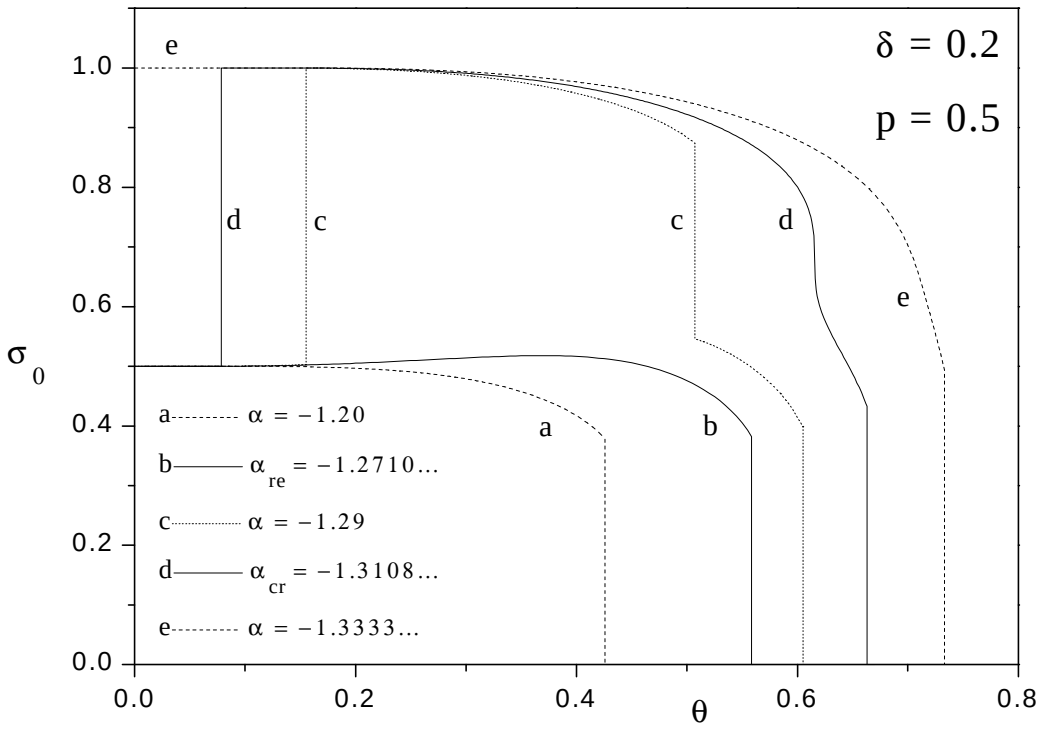

Figure 11

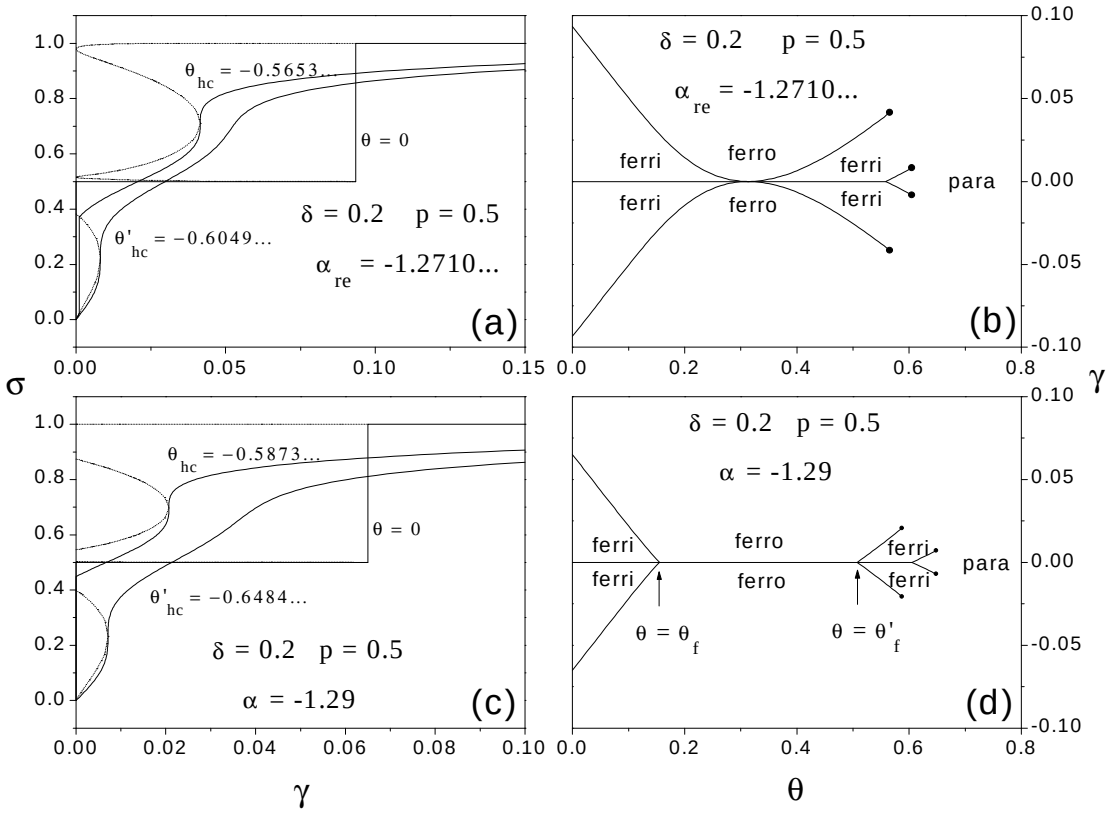
σ
γ
θ
(a)
(b)
(c)
(d)
θ_hc = −0.5653...
θ = 0
θ'_hc = −0.6049...
δ = 0.2 p = 0.5
α_re = -1.2710...
θ_hc = −0.5873...
θ'_hc = −0.6484...
α = -1.29
ferri
ferro
para
θ = θ_f
θ = θ'_f

Figure 12

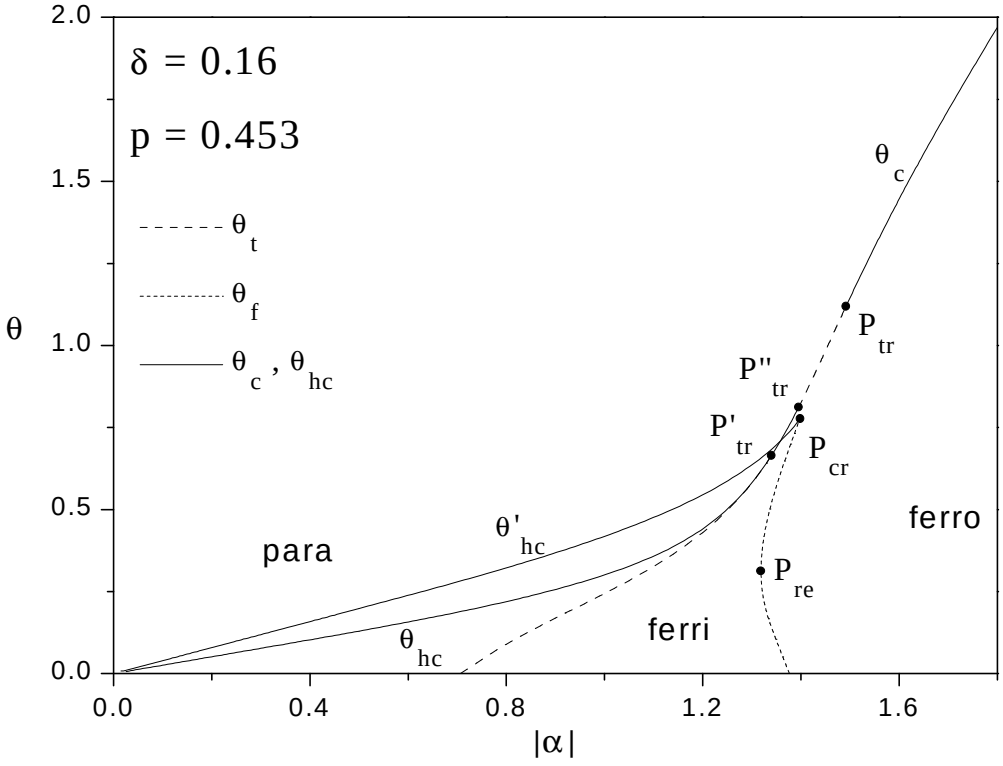
δ = 0.16
p = 0.453
θ_t
θ_f
θ_c , θ_hc
θ_c
P_tr
P''_tr
P'_tr
P_cr
P_re
θ'_hc
θ_hc
para
ferri
ferro
θ
|α|
0.0
0.5
1.0
1.5
2.0
0.0
0.4
0.8
1.2
1.6

Figure 13

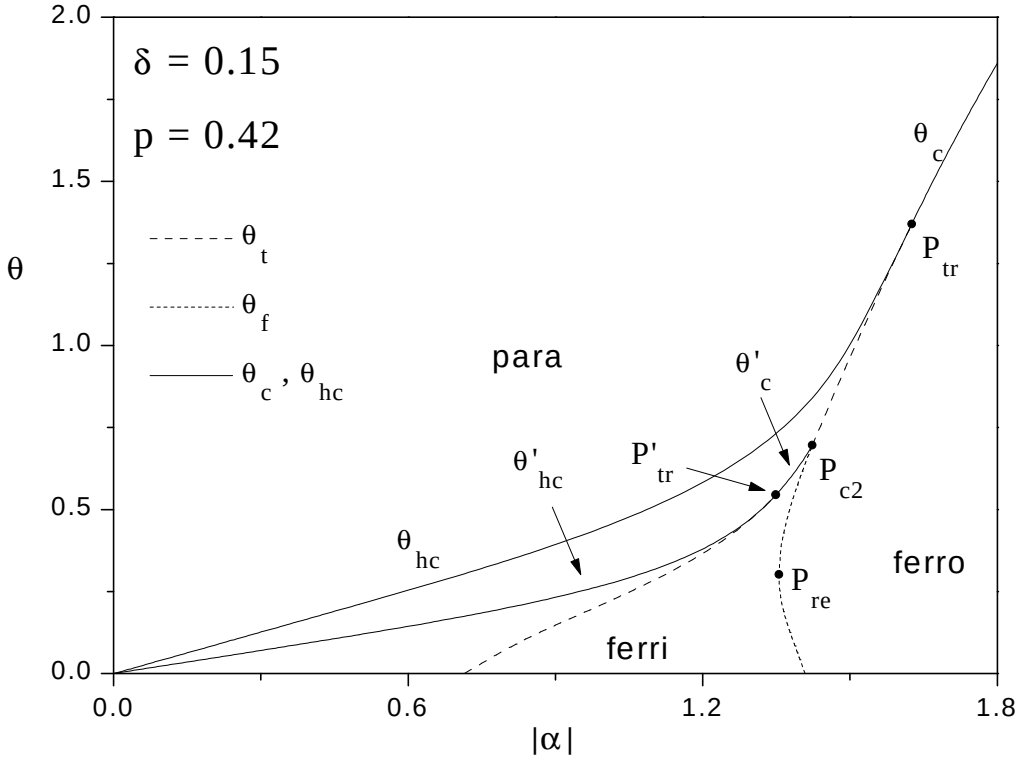
δ = 0.15
p = 0.42
θ
θ_t
θ_f
θ_c , θ_hc
para
ferri
ferro
θ_c
P_tr
θ'_c
θ'_hc
P'_tr
P_c2
θ_hc
P_re
2.0
1.5
1.0
0.5
0.0
0.0
0.6
1.2
1.8
|α|

Figure 14

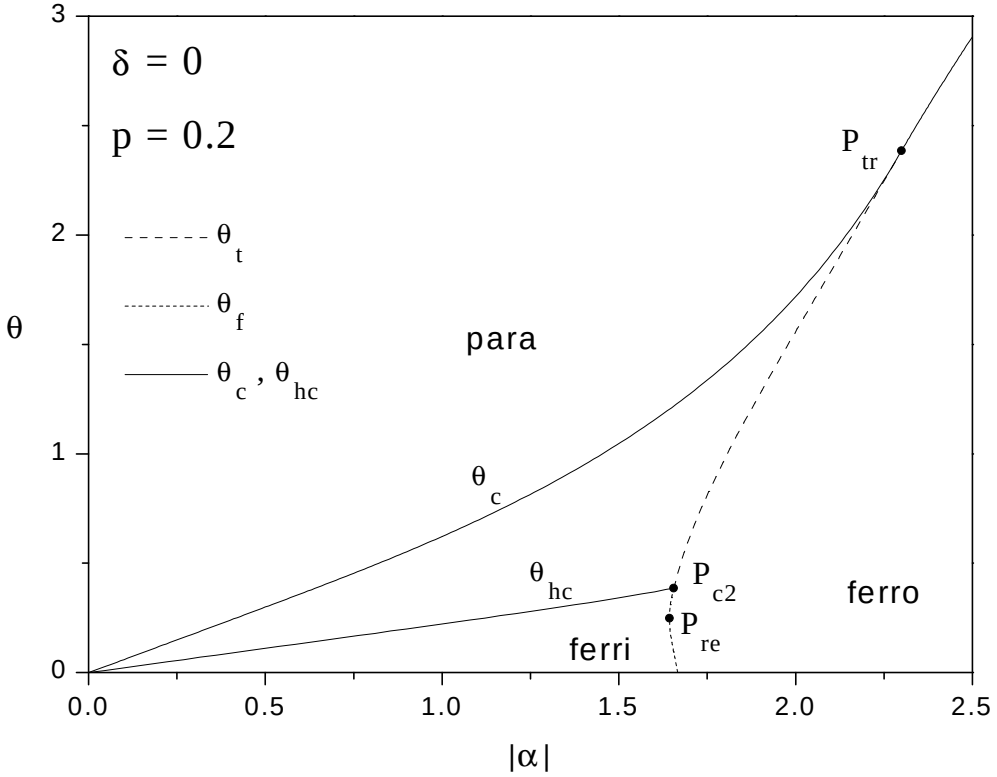
δ = 0
p = 0.2
θ_t
θ_f
θ_c , θ_hc
para
ferro
ferri
θ_c
θ_hc
P_tr
P_c2
P_re
θ
|α|
0
1
2
3
0.0
0.5
1.0
1.5
2.0
2.5

Figure 15

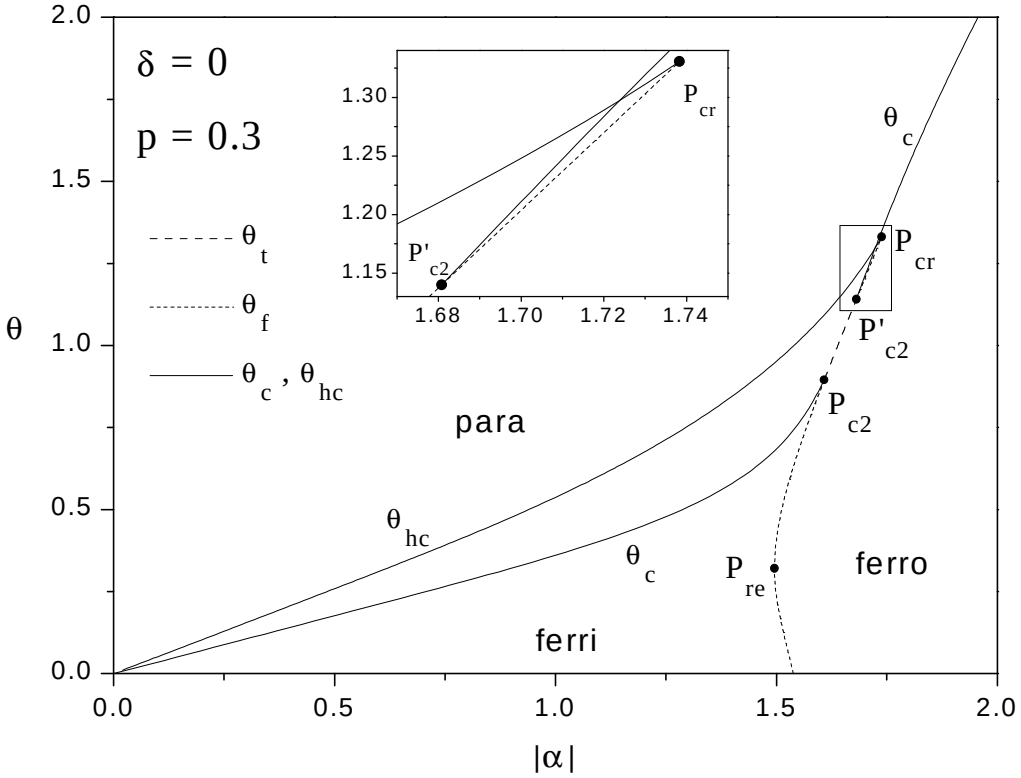
δ = 0
p = 0.3
θ t
θ f
θ c , θ hc
para
ferri
ferro
θ hc
θ c
θ c
P cr
P' c2
P c2
P re
P cr
P' c2
θ
|α|
2.0
1.5
1.0
0.5
0.0
0.0
0.5
1.0
1.5
2.0
1.30
1.25
1.20
1.15
1.68
1.70
1.72
1.74

Figure 16

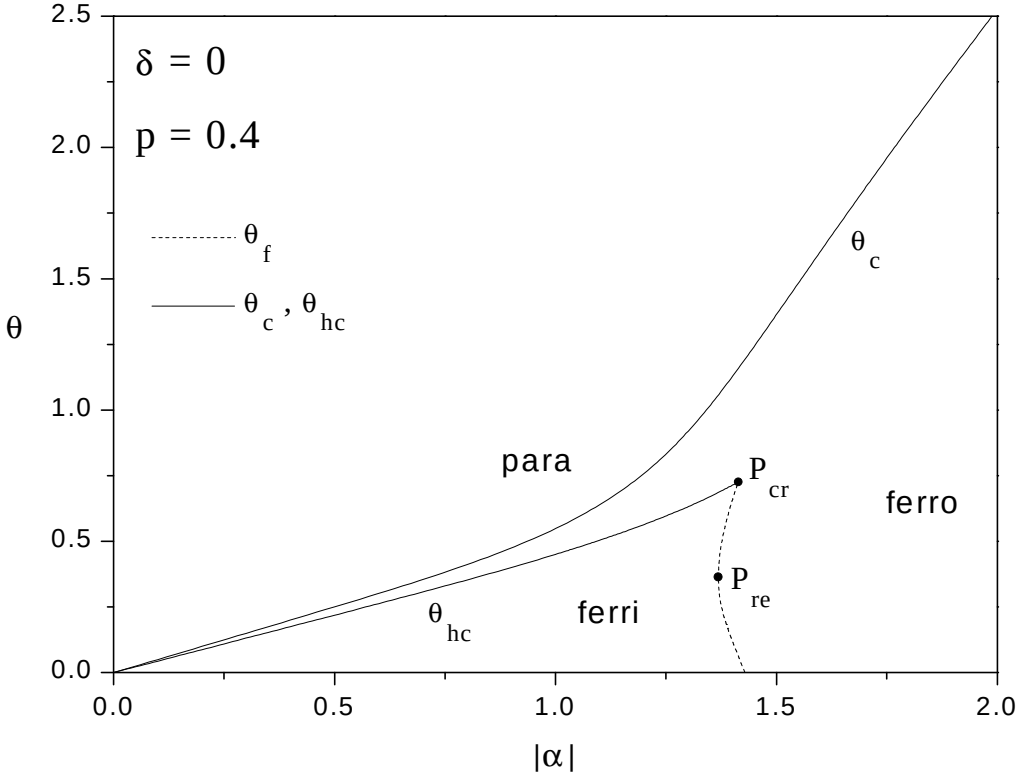
δ = 0
p = 0.4
θ_f
θ_c , θ_hc
θ_c
θ_hc
para
ferri
ferro
P_cr
P_re
θ
|α|
0.0
0.5
1.0
1.5
2.0
2.5

Figure 17

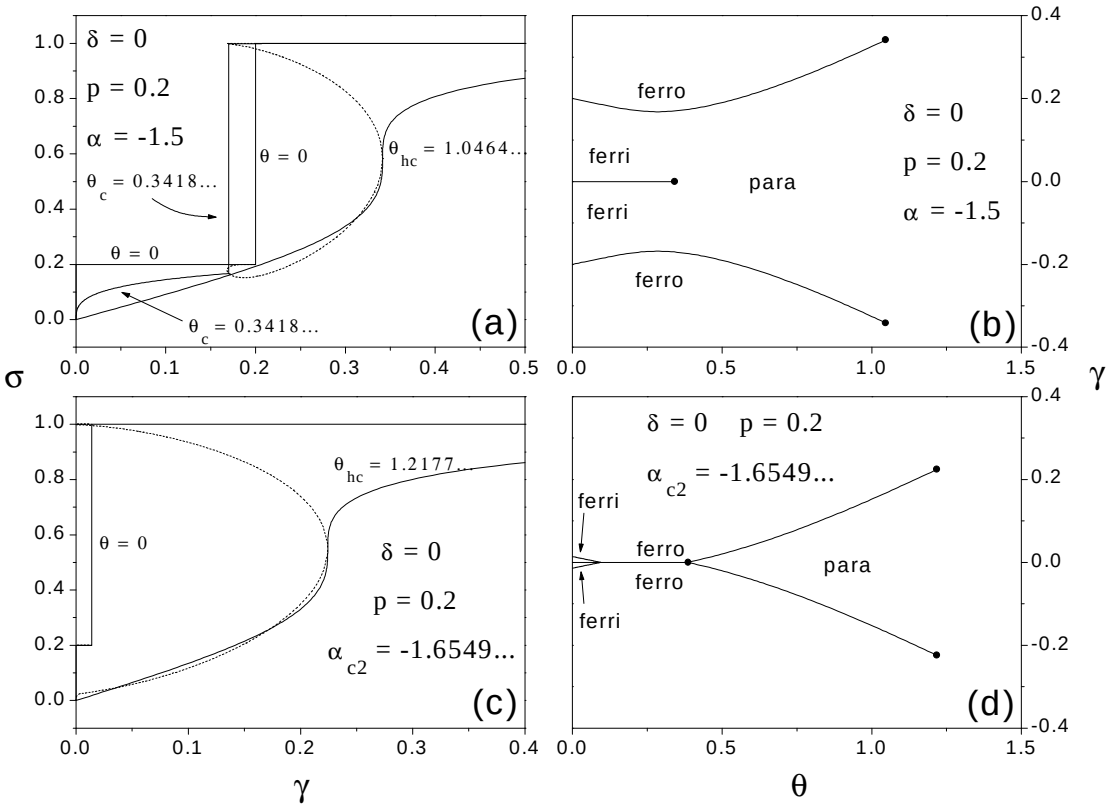
δ = 0
p = 0.2
α = -1.5
θ = 0
θ_hc = 1.0464...
θ_c = 0.3418...
θ = 0
θ_c = 0.3418...
(a)
σ
ferro
ferri
para
ferri
ferro
δ = 0
p = 0.2
α = -1.5
(b)
γ
θ_hc = 1.2177...
θ = 0
δ = 0
p = 0.2
α_c2 = -1.6549...
(c)
γ
δ = 0 p = 0.2
α_c2 = -1.6549...
ferri
ferro
ferro
ferri
para
(d)
θ

Figure 18

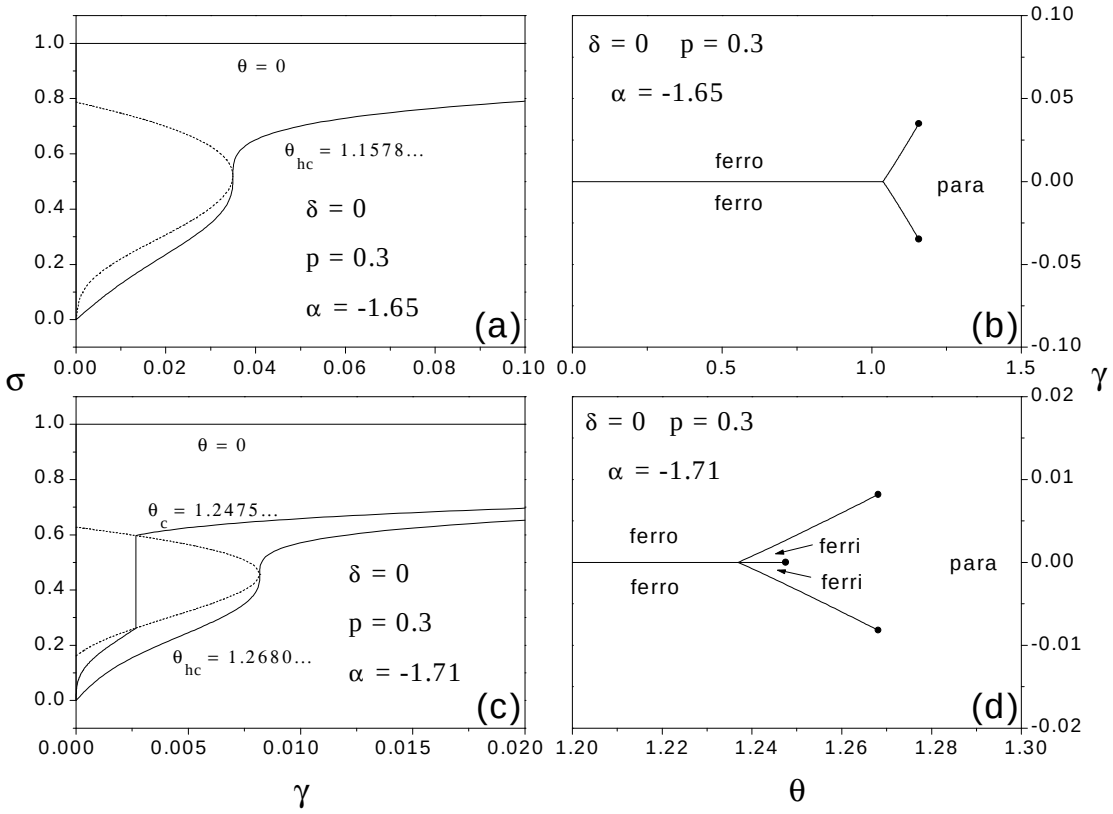
θ = 0
θ hc = 1.1578...
δ = 0
p = 0.3
α = -1.65
(a)
δ = 0 p = 0.3
α = -1.65
ferro
ferro
para
(b)
σ
γ
θ = 0
θ c = 1.2475...
θ hc = 1.2680...
δ = 0
p = 0.3
α = -1.71
(c)
δ = 0 p = 0.3
α = -1.71
ferro
ferro
ferri
ferri
para
(d)
γ
θ

Figure 19